Polymer 166 (2019) 148–154

Contents lists available at ScienceDirect

Polymer

journal homepage: www.elsevier.com/locate/polymer

Short communication

Mechanical energy dissipation in polydomain nematic liquid crystal elastomers in response to oscillating loading

Daniel R. Merkel[a], Rajib K. Shaha[a], Christopher M. Yakacki[b], Carl P. Frick[a,*]

[a] University of Wyoming, Department of Mechanical Engineering, Laramie, WY, USA
[b] University of Colorado Denver, Department of Mechanical Engineering, Denver, CO, USA

HIGHLIGHTS

- Main-chain polydomain nematic liquid crystal elastomers were polymerized in the nematic phase.
- Mechanical properties and relaxation phenomena were studied throughout at broad thermal range.
- Cyclic loading to high stress resulted in efficient energy dissipation (hysteresis) in the rubbery nematic thermal range.

ARTICLE INFO

Keywords:
Liquid crystal elastomers
Thermomechanical properties

ABSTRACT

Liquid crystal elastomers (LCEs) exhibit exotic mechanical behaviors such as reversible actuation, elevated loss tangent above the glass transition, and soft elasticity; however, LCEs have yet to be thoroughly investigated under high-strain cyclic loading. This study explores a main-chain polydomain nematic elastomer synthesized from a thiol-acrylate Michael-addition reaction in the nematic state. Low-strain (i.e., < 0.2%) dynamic mechanical analysis and creep behavior was used to help link viscoelasticity and mesogen reorientation to high-strain cyclic loading. Specifically, the behavior was compared at discrete temperatures below the glass transition, in the nematic-rubbery regime, and in the isotropic-rubbery regime. Creep behavior in the nematic-rubbery regime was modeled using two characteristic relaxation times, which decreased with increasing temperature (τ_1, τ_2 (19 °C) = 140 s, 16 s, and τ_1, τ_2 (62 °C) = 2.4 s, 0.6 s). Samples were repeatedly loaded to 50 kPa at 5 cycles/min at each temperature for 350 cycles. In the rubbery nematic state at 62 °C, low threshold stress and short relaxation times allowed reversible domain reorientation between each cycle, resulting in a repeatable stress-strain curve with high hysteresis (220 kJ/m^3). In contrast, the 19 °C and 39 °C conditions in the rubbery nematic state demonstrated ratcheting behavior in response to cyclic loading, which lowered the hysteresis values with increased cycling. The findings presented here represent the first investigation into mechanical energy dissipation in main-chain nematic LCEs under large oscillating stress conditions. Overall, this study helps to better understand the role LCEs can play in energy dissipating applications with high values of strain and varying temperature.

1. Introduction

The unique combination of rubber elasticity and liquid crystalline behavior found in liquid crystal elastomers (LCEs) gives rise to a broad range of thermomechanical properties such as soft elasticity and shape-actuation [1]. Domain structure, one of the most significant factors governing mechanical behavior, is classified into two broad groups: monodomain and polydomain. Monodomain LCEs are defined by the uniform alignment of liquid crystalline components, called mesogens, that imparts a high degree of anisotropy and reversible shape-actuation [2,3]. Conversely, polydomain LCEs are comprised of many microscopic domains of random mesogen alignment relative to one another that are capable of reorganizing by domain and/or mesogen reorientation in response to mechanical load. Several studies have shown that monotonic tensile loading of polydomain LCEs results in the unique soft or semi-soft deformation in which the polydomain structure evolves towards a monodomain by mesogen and domain reorientation to the tensile axis [4–10]. This phenomenon of mesogen/domain reorientation, in addition to viscous motion of non-mesogenic chains, provides a mechanism to dissipate and absorb applied mechanical

* Corresponding author.
E-mail address: cfrick@uwyo.edu (C.P. Frick).

https://doi.org/10.1016/j.polymer.2019.01.042
Received 19 November 2018; Received in revised form 12 January 2019; Accepted 18 January 2019
Available online 22 January 2019
0032-3861/

energy that is unique to LCEs but has not yet been thoroughly investigated.

Polydomain nematic LCEs are proposed for mechanical energy dissipation owing to the soft elastic effect [11]. For example, the response of nematic LCEs to large-strain repeated loading under isothermal conditions is limited to a single study of side-chain LCEs. Results demonstrated material stiffening under repeated compressive loading due gradual domain reorientation [12]. Other studies investigated energy dissipation in main-chain polydomain nematic LCEs in the context of small strains [4,13]. In these studies, loss tangent (*tan δ*) is used to indicate energy dissipation; however, the small-strain nature of these loading schemes make it unlikely that soft elasticity played a significant role, as larger strains are generally required to induce domain reorientation [14,15]. The direct coupling between mesogen and polymer chains found in main-chain LCEs promises significant energy dissipation capability in response to large-strain mechanical load, which has not previously been demonstrated with respect to repeated loading conditions.

It is important to consider viscoelasticity and the influence of temperature on the time-dependent material response in the context of large repeated deformations. Several investigations demonstrated that LCEs conform to the traditional concepts of viscoelasticity in dynamic mechanical experiments [1,13,16–18]. However, only stress relaxation experiments could show that domain/mesogen reorientation and traditional viscoelastic mechanisms contribute to mechanical response at different time scales [4,19–21]. This implies that the capacity for mechanical energy dissipation resulting from each mechanism should vary with temperature in the thermal range between the glass and isotropic transitions, though this has not been shown explicitly.

This study demonstrates the ability of polydomain nematic main-chain LCEs to dissipate energy under large oscillating mechanical load at discrete temperatures. Mechanisms related to viscoelasticity and domain reorientation were elucidated at various temperatures including the glassy, rubbery nematic, and paranematic thermal ranges. Cycle-by-cycle analysis of set strain progression, average modulus, and hysteresis suggest the presence of more than one dissipation mechanism, which are strongly dependent on temperature. In contrast to previous studies, the results demonstrate reversible deformation mechanisms that do not produce material stiffening at all temperatures. Rather, the response governing energy dissipation in LCEs is dependent on temperature and is most efficient at high temperature in the rubbery nematic regime.

2. Results & discussion

Polydomain nematic main-chain LCEs were fabricated using the thiol-acrylate Michael addition reaction described by Traugutt et al. [22]. When mixed with a base catalyst, mesogenic diacrylates (RM 257), flexible dithiol spacers (EDDET), and flexible tetrathiol crosslinkers (PETMP) assembled into a network of mesogens and spacers composing a main-chain with crosslinker dispersed intermittently (Fig. 1). Thiol-acrylate stoichiometry was balanced such that the reaction consumed equal parts thiol and acrylate functional groups, with 15 mol.% crosslinker. Polymerization took place at room temperature rendering a nematic-polymerized polydomain elastomer, sometimes referred to as nPNE [10], with relatively large domain texture. Previous studies have shown that nPNEs deform by domain reorientation and give relatively short relaxation times compared to the isotropic-polymerized analog [8,10]. Those results indicated that nPNEs might dissipate energy efficiently by reversible domain reorientation under cyclic load; however, this behavior was expected to vary significantly with temperature due to viscoelastic considerations.

Thermomechanical properties including storage modulus (*E′*) and loss tangent (*tan δ*) were investigated by dynamic mechanical analysis (DMA) to elucidate temperature-dependent energy dissipation mechanisms under small cyclic load. Results, shown in Fig. 2a, were

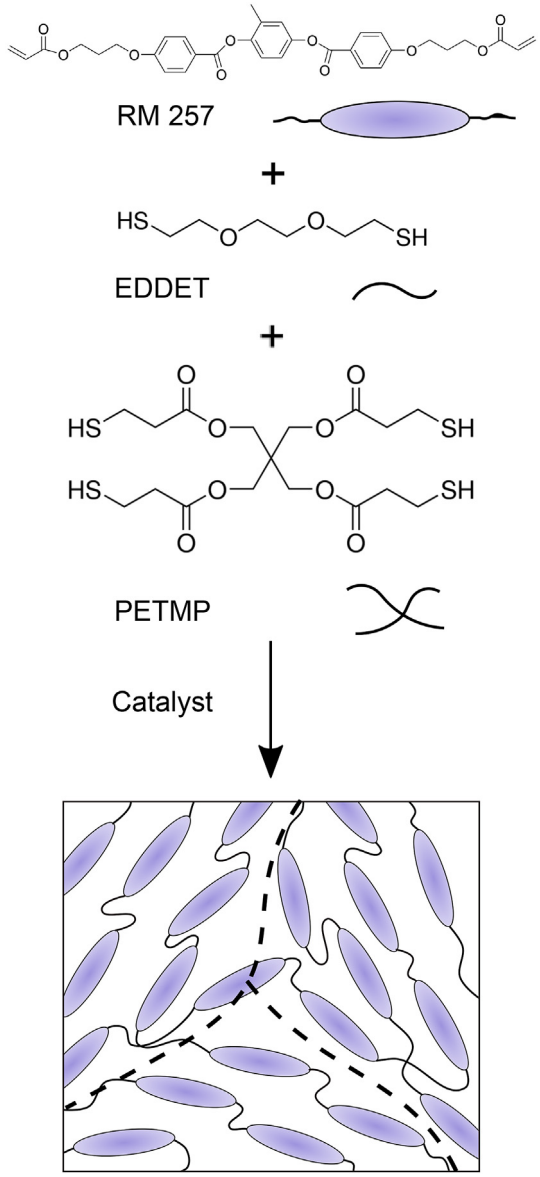

Fig. 1. Nematic LCEs were fabricated by a solvent-less base-catalyzed reaction between diacrylate mesogen (RM 257), dithiol spacer (EDDET), and tetrathiol crosslinker (PETMP). Polymerization resulted in a polydomain nematic LCE with nPNE characteristics. The dashed lines represent domain boundaries.

generally consistent with previous observations [22] demonstrating several thermal ranges with distinct mechanical properties [23]. The glass transition temperature (T_g) at 3 °C and the isotropic transition temperature (T_i) at 76 °C were defined by the low-temperature peak of *tan δ* and the absolute minimum of *E′*, respectively. These characteristic temperatures define thermal ranges in which distinct deformation mechanisms dominate and lead to dissimilar capacity for energy dissipation, indicated by the magnitude of *tan δ*. In the glassy regime below T_g, network deformation was restricted to elastic deformation mechanisms and insignificant energy dissipation indicated by high *E′* and low *tan δ*. Energy dissipation improved above T_g as the network gained mobility and *E'* decreased by several orders of magnitude. In the rubbery nematic range between T_g and T_i, domain rotation and viscous deformation of non-mesogenic segments efficiently dissipated energy, suggested by elevated *tan δ*. At T_i, the network transitioned from the nematic phase, lost domain structure, and behaved similar to an amorphous rubber with limited energy dissipation. A previous study that used the same fabrication technique confirmed paranematic behavior above T_i by X-

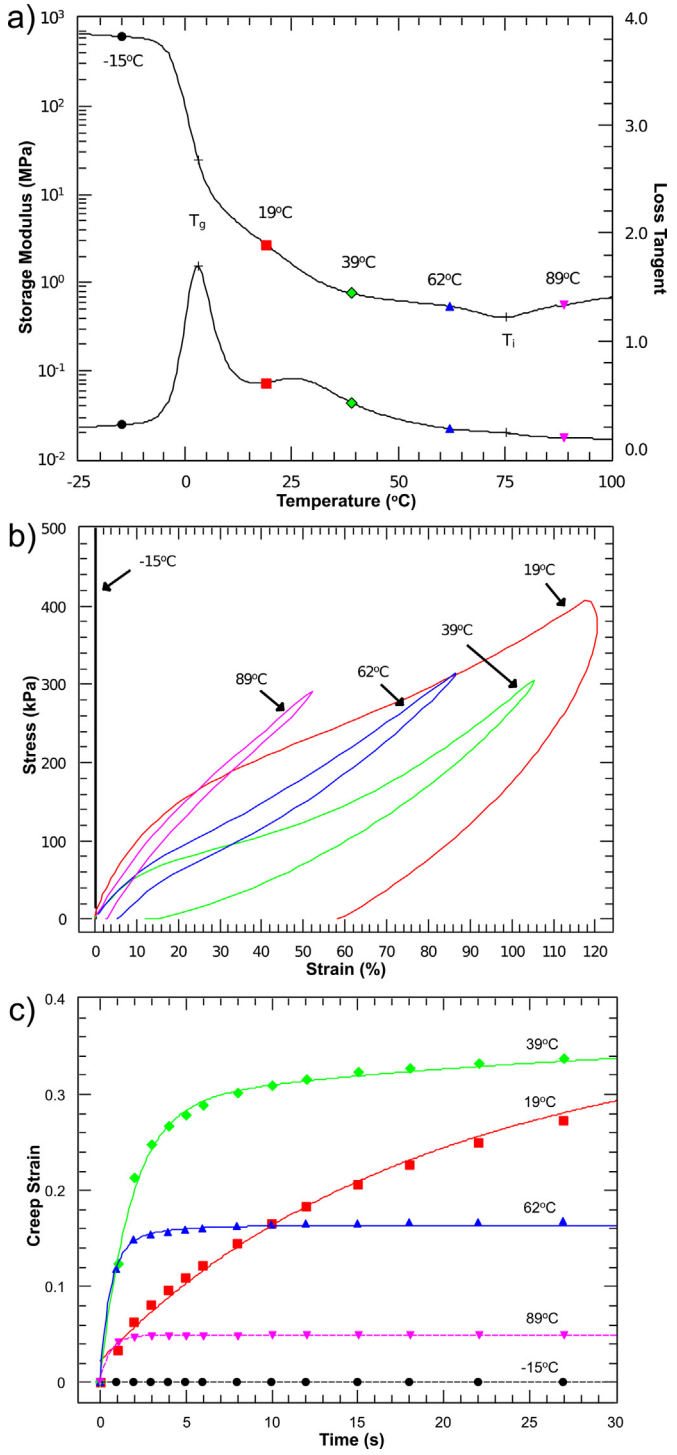

Fig. 2. a) Storage modulus (E') and loss tangent ($tan\ \delta$) curves show the glass transition (T_g) at the maximum of the loss tangent curve and the isotropic transition (T_i) at the minimum of the E' curve. All further testing was performed at discrete temperatures to represent properties in the glassy (−15 °C), rubbery nematic (19 °C, 39 °C, 62 °C), and paranematic (89 °C) ranges. (b) Monotonic tensile loading/unloading at each temperature demonstrated the different responses at each temperature. (c) Creep response to constant 50 kPa tensile load was fit to Equation (1) (dashed lines) or Equation (2) (solid lines) giving characteristic relaxation times at each temperature.

ray scattering analysis [22], which is supported by the broad transition apparent between 65 °C and 85 °C in Fig. 2a [24]. These results demonstrate the potential for efficient energy dissipation throughout the rubbery nematic regime, but are limited to small amplitude loads that may not fully capture mesogen/domain reorientation as a dissipative mechanism.

Mechanical response to larger loads was further examined at discrete temperatures in the glassy (−15 °C), rubbery nematic (19 °C, 39 °C, & 62 °C), and paranematic (89 °C) thermal ranges to elucidate deformation mechanisms. At each temperature in the rubbery nematic range (19 °C, 39 °C, and 62 °C), tensile loading at 400 kPa/min (Fig. 2b) elicited three regimes defining the underlying mechanisms of deformation according to literature [4–10]: (I) initially, loading proceeded linearly as network components extended elastically under tensile load. (II) Beyond a threshold point, a semi-soft region developed defined by a significant reduction in slope associated with a transition from polydomain to monodomain texture. During this polydomain-monodomain transition, the domains reoriented toward alignment with the tensile axis. The slope in regime (II) remained relatively high due to the continuously increasing applied load required to accommodate domain reorientation. This contrasts with LCEs polymerized in the isotropic phase (iPNEs) that exhibit near-zero slope as domains reorient to the tensile axis, called the soft elastic plateau. The dissimilarity stems from a difference in domain size, which has previously been shown to be significantly larger in nPNEs like the ones studied in this article [10]. (III) Elastic network extension resumed with increasing slope as domains reached maximum alignment with the tensile axis. At high extension, the nPNE remained optically semi-opaque indicating that domains were not fully aligned with the tensile axis, which is characteristic of nPNEs. Azoug et al. [4] previously showed temperature-dependent variations in the onset of deformation regimes (I), (II), and (III) of an iPNE of similar chemistry. The nPNE studied in this article demonstrated like temperature-dependence; the threshold point for the transition from region (I) to region (II) decreased from 190 kPa to 33% strain at 19 °C to 30 kPa and 5% strain at 62 °C, demonstrating a significant decrease in the load required to initiate widespread domain reorientation. In a previous study on nPNEs fabricated by the same method, Traugutt et al., demonstrated strain-induced change to the domain structure by polarized light microscopy, confirming widespread domain reorientation due to tensile extension [22]. Threshold stress and strain values were calculated by a 50% departure from a tangent to the semi-soft slope for each temperature in the rubbery nematic regime and are tabulated in Table 1. Fig. 2b also showed large areas enclosed by the loading and unloading curves at each temperature in the rubbery nematic range along with non-zero residual strain after unloading to zero stress. This indicated significant energy dissipation due to inelastic viscous deformation and domain reorientation mechanisms.

The viscoelastic nature of each mechanism was further elucidated by creep testing at each temperature to better understand the respective contributions of each mechanism to total deformation of the LCE. Creep relaxation times were estimated by fitting exponential functions to creep data obtained under constant applied stress of 50 kPa for up to 60 min at each temperature. The first 30 s of creep results are reported in Fig. 2c. An exponential decay function (Equation (1)) derived from the Kelvin-Voigt model is commonly used to elucidate relaxation times of viscoelastic polymers [23,25–27] by fitting creep strain to a characteristic relaxation time. However, this model was inadequate in the rubbery nematic range where the summation of two decay functions (Equation (2)) was required to obtain an accurate fit. This was

Table 1
Compilation of data from tensile and creep tests.

Temperature (°C)	Threshold Stress (kPa)	Threshold strain (%)	τ_1 (s)	τ_2 (s)
−15	–	–	830	–
19	190	33	140	16
39	80	19	29	1.8
62	30	5	2.4	0.6
89	–	–	0.6	–

attributed to the presence of two different relaxation mechanisms in this temperature range. Both relaxation times trended toward shorter time scales with increasing temperature (Table 1) due to increased network and domain mobility, which is consistent with traditional viscoelastic principles. Approximately one order of magnitude difference was maintained between relaxation times at each temperature within the rubbery nematic regime. The longer relaxation time ranged from 140 s to 2.4 s while the shorter relaxation time ranged from 16 s to 0.6 s over the temperature interval from 19 °C to 62 °C. Creep rate, shown in Fig. 2c, demonstrated a corresponding trend, reaching steady-state after about 60 min at 19 °C and after 27 s at 62 °C. These results suggest that viscous deformations and domain reorientation are separate, but not independent, relaxation mechanisms, which is supported by the literature [1,4,5,20,28,]. This study did not attempt to assign a specific mechanism to each relaxation time, although previous studies have proposed domain/mesogen reorientation and traditional polymer mechanisms as the short and long time scale phenomena, respectively, in side-chain nematic LCEs [19,20]. These results indicate that the two mechanisms can be leveraged to efficiently dissipate energy under cyclic loading at an appropriate temperature and loading scheme. However, the longer of the two relaxation times could be detrimental to energy dissipation, especially in the high-frequency domain where the cycle time is significantly shorter than the relaxation time. The steady-state strain values for 19 °C, 39 °C, and 62 °C were 52%, 36%, and 16%, respectively.

In contrast to creep behavior in the rubbery nematic range, mechanical responses in the glassy and paranematic thermal ranges were straightforward, demonstrating rigid elastic deformation at −15 °C and rubbery elastic deformation at 89 °C. Neither condition showed evidence of domain reorientation and was simply fit by the traditional creep relaxation model (Equation (1)) with a single relaxation time. Long relaxation time on the order of 830 s was characteristic of the glassy range. Creep strain reached less than 1% after 30 min of constant applied stress. The paranematic range showed the fastest creep rate, reaching the steady-state of 5% strain within 3 s, and a relatively short relaxation time of 0.6 s, which was comparable to the fastest characteristic time observed at 62 °C.

The ability of LCEs to efficiently dissipate energy in response to large cyclic loads was evaluated at each temperature under an applied stress amplitude of 50 kPa. The loading scheme followed a triangle-wave with 5 cycles/min frequency. This loading scheme was selected to highlight the influence of domain reorientation under large amplitude loads. Previous studies were restricted to low amplitude DMA investigations, which do not emphasize domain reorientation as a dissipative mechanism. Stress-strain plots of several cycles are shown in Fig. 3a for each temperature. Hysteresis and set strain (i.e., the strain upon unloading), which were measured during each cycle, reached steady-state values shown in Fig. 3b. Hysteresis, a measure of large-strain energy dissipation, was evaluated as the area enveloped by the stress-strain loops generated during each cycle. This data is also represented on a cycle-by-cycle basis in Fig. S1 and Fig. S2 of the Supporting Information.

Cycling in the rubbery nematic range produced stress-strain cycle loops (Fig. 3a) indicating significant hysteretic energy dissipation with each cycle. The contributions of viscous deformations and domain reorientation to energy dissipation varied at each temperature and, in some cases, changed with continuous cycling before reaching a steady-state. This was evident in the shape of the stress-strain loops and dissimilarity in set strain at each temperature (Fig. 3b) as well as cycle-by-cycle analyses of hysteresis and average modulus (Fig. S1 and Fig. S3). Average modulus captured the relative stiffness of the LCE during each cycle and was calculated by Equation (3) [25].

Cycling at 19 °C demonstrated the effect of long relaxation times on energy dissipation during cyclic loading. The cycle time was significantly shorter than either relaxation time elucidated from creep testing. Consequently, stress relaxation was evident at the maximum of each loop where stress decreased as strain continued to increase. The inverse stress-strain relationship was observed at the minimum of each loop. The long relaxation time also caused an accumulation of 80% set strain after about 300 cycles, shown in Fig. S2. Hysteretic energy dissipation was comparable to values observed at each condition in the rubbery nematic range (Fig. 3b); however, a unique trend in hysteresis

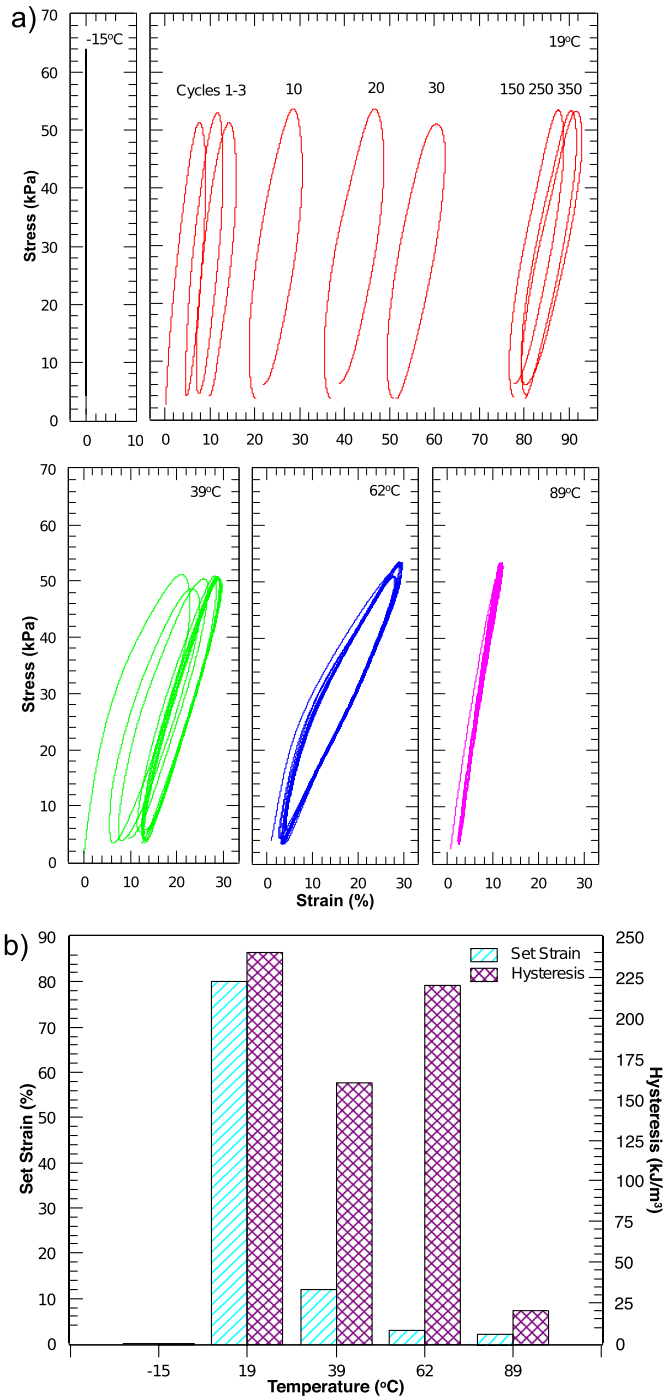

Fig. 3. (a) Stress-strain loops generated during cyclic loading. Cycles 1–3, 10, 20, 30, 150, 250, and 350 are shown for each temperature. (b) Steady-state set strain and hysteresis were calculated from cyclic tests. Set strain, the semi-permanent deformation observed at the start of each cycle after steady-state was reached, was highest at 19 °C and decreased dramatically at higher temperature. Hysteresis, representing energy dissipation in each cycle after steady-state was reached, was significant in the rubbery nematic range. Cycle-by-cycle analysis of hysteresis and set strain are shown in the Supporting Information.

was observed in a cycle-by-cycle analysis shown in Fig. S1. The dissipative mechanism was dominated by viscous deformation through 350 cycles, except a period of about 50 cycles near the start of the experiment. As shown in Fig. 3a, the first 3 cycles showed linear stress-strain relationships during the loading strokes with negligible strain recovery upon unloading. Deformation in these first few cycles was due to traditional viscoelastic mechanisms; however, hysteresis increased with each cycle from about 240 kJ/m^3 in the first cycle to a maximum of about 350 kJ/m^3 in cycle 15. The cause of this rapid increase in hysteresis was an increasingly significant contribution of unrecovered domain reorientation to the total deformation of the LCE. This caused modulus to decrease in the first 15 cycles (Fig. S3) as domain reorientation became the prevalent deformation mechanism, akin to the tensile transition from region (I) to region (II) shown in Fig. 2b. Beyond cycle 15, the trend reversed as domains became oriented towards the tensile axis and hysteresis reached steady-state at about 240 kJ/m^3. This was the highest steady-state hysteresis observed in this study. Modulus increases slightly from the minimum at cycle 15 to reach the steady-state value, consistent with the tensile transition to region (III). Although energy dissipation at this temperature was significant, the accumulated set strain produced a large deformation that would be disadvantageous in mechanical damping applications.

Cycling at 39 °C resulted in set strain accumulation reaching a steady-state of 12% by cycle 10, which was a significant decrease compared to the 19 °C condition (Fig. 3b). Stress-strain loops showed a dramatic change in shape in the first few cycles (Fig. 3a) during which the cycle loop narrowed, reducing the encompassed area. This generated a single-cycle hysteresis of 500 kJ/m^3 in the first cycle (Fig. S1), the highest observed in this study, but rapidly decreased to 160 kJ/m^3 as domains gradually reoriented toward the tensile axis with each subsequent loading stroke. Modulus increased in the first few cycles, consistent the transition from region (II) to region (III) of tensile experiments. Thus, domain reorientation was the dominant energy dissipation mechanism in the first few cycles but diminished as domains reoriented. Despite the reduction in set strain compared to the 19 °C condition, energy dissipation was also significantly reduced as shown in Fig. 3b.

At 62 °C, low threshold stress and short relaxation times allowed reversible domain reorientation with each cycle. In contrast to the 19 °C and 39 °C conditions, cycle loops maintained the same shape throughout the experiment (Fig. 3a), demonstrating non-linear elastic deformation and recovery with each cycle. Energy dissipated by reversible domain reorientation produced steady-state hysteresis of 220 kJ/m^3 with set strain limited to just 3% (Fig. 3b), which resulted from the first cycle only. Energy dissipation at this temperature was significantly improved over the 39 °C condition while set strain was greatly reduced compared to the 19 °C and 39 °C conditions. Modulus maintained a relatively low value of 200 kPa, suggesting domain reorientation was entirely reversed in each cycle (Fig. S3). This contrasts sharply with the continuous dynamic stiffening of side-chain nematic LCEs observed by Agrawal et al. [12]. In that study, mesogens gradually reoriented toward the neutral axis with each cycle resulting in stiffening of the LCE with continuous cycling.

In the paranematic range (89 °C), the LCE behaved similarly to an amorphous rubber with negligible hysteretic energy dissipation. The first cycle produced a set strain of about 2% that did not increase with further cycling. This observation is reminiscent of the Mullins effect commonly observed in filled and crystallizing rubbers [29], although the LCE presented in this study did not contain fillers nor has it shown crystallinity [22]. This phenomenon may also explain the set strain produced in the first cycle at 62 °C. Hysteresis in the first cycle was about 80 kJ/m^3 resulting from the set strain of the first cycle. By the second cycle, hysteresis reached the steady-state of 20 kJ/m^3, which was insignificant compared to the values observed in the rubbery nematic range. Highly elastic behavior of the glassy range (−15 °C) demonstrated negligible energy dissipation value.

Energy dissipation under the high amplitude, low-frequency loading scheme was clearly improved by domain reorientation; however, performance may be further improved by optimizing the LCE microstructure. Several recent papers on LCEs with similar chemistry have demonstrated the importance of monomer selection and stoichiometry on thermomechanical properties [30,31,32–34]. Likewise, domain structure can be tuned by the use of a solvent [22] or temperature during synthesis to further influence mechanical response such as relaxation time [21]. This study used a loading frequency on the order of the longest relaxation time observed at 62 °C, which showed excellent energy dissipation. However, this performance is not expected at higher frequencies, which is a critical limitation for vibration damping applications. Therefore, future efforts will attempt to reduce relaxation time by control of the LCE microstructure. Alternatively, reversible domain reorientation could be forced by tension-compression cyclic loading scheme rather than the tension-tension scheme demonstrated in this article. These investigations are ongoing.

3. Conclusions

The findings presented here represent the first investigation into mechanical energy dissipation in main-chain nematic LCEs under large oscillating stress conditions. Viscoelasticity and domain reorientation, which contribute to energy dissipation, were first investigated by monotonic tensile tests and creep experiments. Tensile tests in the rubbery nematic thermal range elicited classic polydomain nPNE responses with semi-soft plateaus. Threshold stress and strain marking the onset of widespread domain reorientation decreased from 190 kPa and 33% strain to 30 kPa and 5% strain with a temperature increase from 19 °C to 62 °C. Thus, load required to induce domain reorientation decreased at higher temperature. Creep experiments in the rubbery nematic thermal range demonstrated two deformation mechanisms with separate relaxation times at each temperature. The longest relaxation time decreased from 150 s to 2.4 s while the shortest relaxation time decreased from 18 s to 0.6 s with increasing temperature from 19 °C to 62 °C. This result indicated faster recovery of the original polydomain texture after unloading from a deformed state. Cyclic tests showed excellent energy dissipation at 19 °C indicated by steady-state hysteresis of 240 kJ/m^3; however, this came at the expense of set strain accumulation up to 80% due to progressive domain reorientation toward the tensile axis with each cycle. At 62 °C, both recovery times were shorter than the cycle time, allowing domains to reorient reversibly in each cycle. This deformation mechanism produced a high steady-state hysteresis of 220 kJ/m^3 without set strain accumulation. These results indicate a reversible deformation mechanism that dissipates energy efficiently at high temperatures within the rubbery nematic regime without performance loss over hundreds of cycles.

4. Materials and methods

4.1. Materials

4-bis-[4-(3-acryloyloxypropypropyloxy) benzoyloxy]-2-methylbenzene (CAS: 174063-87-7) (RM257) was purchased from Wilshire Technologies, Inc. (Princeton, NJ, USA). Pentaerythritol tetra (3-mercaptopropionate) (PETMP), 2,2-(ethylenedioxy) diethanethiol (EDDET), 2,6-di-tert-butyl-4-methylphenol (BHT), and triethylamine (TEA) were purchased from Sigma-Aldrich, Inc. (St. Louis, MO, USA). All materials were used as-received without further purification.

4.2. Liquid crystal elastomer fabrication

Main-chain liquid crystal elastomers were synthesized by a method adapted from the literature [22]. Stoichiometric balance of acrylate functional (RM 257) groups relative to thiol functional groups was maintained to ensure high conversion. The amount of crosslinker

(PETMP) (15 mol.%) was calculated by the number thiol functional groups contributed by crosslinker relative to the total number of thiol groups from crosslinker and spacer (EDDET).

RM257 and BHT (1.5 wt %) were melted and mixed with EDDET and PETMP monomers. TEA (0.33 wt%) was added to the reaction mixture to initiate a thiol-acrylate Michael addition reaction. The solution was degassed under 21 in-Hg vacuum and cast between two glass slides with 1 mm polytetrafluoroethylene spacers between slides. The mixture polymerized overnight at room temperature forming an opaque white elastomer, indicating a liquid crystalline phase in the polydomain conformation.

4.3. Dynamic mechanical properties

Dynamic mechanical properties including storage modulus (E') and loss tangent ($tan\ \delta$) were investigated with a dynamic mechanical analyzer (DMA Q800, TA Instruments, New Castle, DE, USA) in DMA strain control mode using tensile grips. LCEs approximately 7 mm wide and 1 mm thick were clamped with 10 mm between grips, thermally cycled into the paranematic thermal range, cooled to subambient temperature, and allowed to reach thermal equilibrium for 10 min prior to starting each test. All tests were performed at 0.2% strain amplitude, 0.01 N preload force, and 1 Hz oscillating frequency. Temperature was ramped up at 0.5 °C/min to maintain uniform temperature through the thickness of each sample. The glass transition temperature (T_g) was determined at the peak of the $tan\ \delta$ curve while the paranematic transition temperature (T_i) as taken at the minimum of the E' curve.

4.4. Tensile response

LCEs measuring approximately 10 mm wide by 1 mm thick were clamped in the Q800 DMA and uniaxially extended in controlled force mode at a constant rate of 4 N/min to resolve the stress-strain behavior of the sample. Threshold stresses for each temperature were evaluated at the points where the stress-strain curve deviated by 50% from the slope of second linear regime (semi-soft regime). The threshold stresses indicated onset of the polydomain-monodomain transition in which widespread domain reorientation was the primary deformation mechanism. Unloading and elastic recovery behavior was obtained by reducing force to 0 N at 4 N/min from a predetermined load corresponding to a point beyond the second linear regime. When no threshold point was detectable, such as at −15 °C or 89 °C, samples were unloaded from points of high load.

4.5. Creep testing

Viscoelastic behavior was evaluated by creep testing under constant applied stress of 50 kPa for up to 1 h. Relaxation time was estimated by fitting creep data to an exponential decay function (Equation (1) and Equation (2)) where τ represents relaxation time.

$$\varepsilon(t) \sim e^{-t/\tau} \tag{1}$$

$$\varepsilon(t) \sim e^{-t/\tau_1} + e^{-t/\tau_2} \tag{2}$$

4.6. Cyclic loading

LCEs measuring approximately 10 mm wide by 1 mm thick were cyclically loaded in a tension-tension scheme with a minimum stress of 1 kPa and a maximum stress of 55 kPa for all temperatures. Loading was carried out with the Q800 DMA in controlled force mode with a ramp rate of 4 N/min in triangle-wave fashion *(i.e.,* linear loading up and down) at a frequency of 5 cycles/min. This loading scheme allowed sufficient data for individual cycles to be observed, which was necessary for analyzing changes in thermomechanical properties over time. Residual strain was evaluated as the minimum strain observed in each cycle. Average modulus (E_{avg}) was calculated by Equation (3) for each cycle. The energy dissipated by each cycle was evaluated by the area enclosed by each loop, representing hysteresis.

$$E_{avg} = \frac{\sigma_{max} - \sigma_{min}}{\varepsilon_{max} - \varepsilon_{min}} \tag{3}$$

Conflicts of interest

CMY and CPF have a financial interest in Impressio Inc., a company involved with the commercialization of liquid crystal elastomers.

Funding sources

CPF appreciates support from an Institutional Development Award (IDeA) from the National Institute of General Medical Sciences of the National Institutes of Health under Grant No. 2P20GM103432 and NSF-PFI Grant No. 1827288. CMY thanks the National Science Foundation Faculty Early Career Development Program. CMY acknowledges this material is based upon work supported by, or in part by, the U.S. Army Research Laboratory and the U.S. Army Research Office under grant number W911NF1710165 as well as the National Science Foundation CAREER award CMMI-1350436.

Acknowledgements

The authors would like to thank Jason Young for specimen fabrication and preliminary testing and Isaac Ruse for equipment set-up and calibration.

Appendix A. Supplementary data

Supplementary data to this article can be found online at https://doi.org/10.1016/j.polymer.2019.01.042.

References

[1] M. Warner, E.M. Terentjev, Liquid Crystal Elastomers, Oxford University Press, 2007.
[2] Ruvini S. Kularatne, Hyun Kim, Jennifer M. Boothby, Taylor H. Ware, Liquid crystal elastomer actuators: synthesis, alignment, and applications, J. Polym. Sci. B Polym. Phys. 55 (5) (2017) 395–411, https://doi.org/10.1002/polb.24287.
[3] Christian Ohm, Martin Brehmer, Rudolf Zentel, Liquid crystalline elastomers as actuators and sensors, Adv. Mater. 22 (31) (2010) 3366–3387, https://doi.org/10.1002/adma.200904059.
[4] A. Azoug, V. Vasconcellos, J. Dooling, M. Saed, C.M. Yakacki, T.D. Nguyen, Viscoelasticity of the polydomain-monodomain transition in main-chain liquid crystal elastomers, Polymer 98 (2016), https://doi.org/10.1016/j.polymer.2016.06.022 (August). Elsevier Ltd: 165–71.
[5] S.M. Clarke, E.M. Terentjev, I. Kundler, H. Finkelmann, Texture evolution during the polydomain-monodomain transition in nematic elastomers, Macromolecules 31 (15) (1998) 4862–4872, https://doi.org/10.1021/ma980195j.
[6] Sonal Dey, Dena Agra-Kooijman, Wanting Ren, Philip McMullan, Anselm Griffin, Satyendra Kumar, Soft elasticity in main chain liquid crystal elastomers, Crystals 3 (2) (2013) 363–390, https://doi.org/10.3390/cryst3020363.
[7] S.V. Fridrikh, E.M. Terentjev, Polydomain-monodomain transition in nematic elastomers, Phys. Rev. 60 (2) (1999) 1847–1857, https://doi.org/10.1103/PhysRevE.60.1847.
[8] Haruko Higaki, Kenji Urayama, Toshikazu Takigawa, Memory and development of textures of polydomain nematic elastomers, Macromol. Chem. Phys. 213 (18) (2012) 1907–1912, https://doi.org/10.1002/macp.201200239.
[9] Gregor Skačej, Claudio Zannoni, Molecular simulations shed light on supersoft elasticity in polydomain liquid crystal elastomers, Macromolecules 47 (24) (2014) 8824–8832, https://doi.org/10.1021/ma501836j.
[10] Kenji Urayama, Etsuko Kohmon, Masahiro Kojima, Toshikazu Takigawa, "Polydomain−Monodomain transition of randomly disordered nematic elastomers with different cross-linking histories, Macromolecules 42 (12) (2009) 4084–4089, https://doi.org/10.1021/ma9004692.
[11] S.M. Clarke, A.R. Tajbakhsh, E.M. Terentjev, C. Remillat, G.R. Tomlinson, J.R. House, Soft elasticity and mechanical damping in liquid crystalline elastomers, J. Appl. Phys. 89 (11) (2001) 6530–6535, https://doi.org/10.1063/1.1368177.
[12] Aditya Agrawal, Alin C. Chipara, Yousif Shamoo, Prabir K. Patra, Brent J. Carey, Pulickel M. Ajayan, Walter G. Chapman, Rafael Verduzco, Dynamic self-stiffening in liquid crystal elastomers, Nat. Commun. 4 (2013), https://doi.org/10.1038/ncomms2772 Nature Publishing Group: 1739.

[13] Marta Giamberini, Veronica Ambrogi, Pierfrancesco Cerruti, Cosimo Carfagna, Viscoelasticity of main chain liquid crystalline elastomers, Polymer 47 (13) (2006) 4490–4496, https://doi.org/10.1016/j.polymer.2006.04.021.
[14] P. Martinoty, P. Stein, H. Finkelmann, H. Pleiner, H.R. Brand, Mechanical properties of mono-domain side chain nematic elastomers, Europ. Phys. J. 14 (4) (2004) 311–321, https://doi.org/10.1140/epje/i2003-10154-y.
[15] E.M. Terentjev, M. Warner, Linear hydrodynamics and viscoelasticity of nematic elastomers, Europ. Phys. J. 4 (3) (2001) 343–353, https://doi.org/10.1007/s101890170117.
[16] J.L. Gallani, L. Hilliou, P. Martinoty, F. Doublet, M. Mauzac, Mechanical behavior of side-chain liquid crystalline networks, J. Phys. II 6 (3) (1996) 443–452, https://doi.org/10.1051/jp2:1996190.
[17] A. Hotta, E.M. Terentjev, Dynamic soft elasticity in monodomain nematic elastomers, Eur. Phys. J. E (EPJ E),Europ. Phys. J. - Soft Matter 10 (4) (2003) 291–301, https://doi.org/10.1140/epje/i2002-10005-5.
[18] P. Stein, N. Aßfalg, H. Finkelmann, P. Martinoty, Shear modulus of polydomain, mono-domain and non-mesomorphic side-chain elastomers: influence of the nematic order, Europ. Phys. J. 4 (3) (2001) 255–262, https://doi.org/10.1007/s101890170107.
[19] S.M. Clarke, E.M. Terentjev, Slow stress relaxation in randomly disordered nematic elastomers and gels, Phys. Rev. Lett. 81 (20) (1998) 4436–4439, https://doi.org/10.1103/PhysRevLett.81.4436.
[20] A. Hotta, E.M. Terentjev, Long-time stress relaxation in polyacrylate nematic liquid crystalline elastomers, J. Phys. Condens. Matter 13 (50) (2001) 11453–11464, https://doi.org/10.1088/0953-8984/13/50/305.
[21] Kenji Urayama, Seiji Honda, Toshikazu Takigawa, Slow dynamics of shape recovery of disordered nematic elastomers, Phys. Rev. E - Stat. Nonlinear Soft Matter Phys. 74 (4) (2006) 1–7, https://doi.org/10.1103/PhysRevE.74.041709.
[22] N.A. Traugutt, R.H. Volpe, M.S. Bollinger, M.O. Saed, A.H. Torbati, K. Yu, Natalia Dadivanyan, C.M. Yakacki, Liquid-crystal order during synthesis affects main-chain liquid-crystal elastomer behavior, Soft Matter 13 (39) (2017) 7013–7025, https://doi.org/10.1039/C7SM01405H.
[23] E. Riande, R. Diaz-Calleja, M. Prolongo, R. Masegosa, C. Salom, Polymer viscoelasticity: stress and strain in practice, Plast. Eng. (2000) 55 New York: Marcel Dekker.
[24] Andrija Lebar, Cordoyiannis George, Zdravko Kutnjak, Boštjan Zalar, The isotropic-to-nematic conversion in liquid crystalline elastomers, in: W.H. de Jeu (Ed.), Liquid Crystalline Elastomers: Materials and Applications, 2012 147–85. Springer http://link.springer.com/10.1007/12_2010_103.
[25] Thomas H. Courtney, Mechanical Behavior of Materials, Waveland Press, 2005.
[26] J.M.G. Cowie, V. Arrighi, Polymers: Chemistry and Physics of Modern Materials, third ed., Chapman and Hall, Inc, New York, 2008.
[27] Nishant Lakhera, Annalena Graucob, Andreas S. Schneider, Elmar Kroner, Eduard Arzt, Christopher M. Yakacki, Carl P. Frick, Effect of viscoelasticity on the spherical and flat adhesion characteristics of photopolymerizable acrylate polymer networks, Int. J. Adhesion Adhes. 44 (2013), https://doi.org/10.1016/j.ijadhadh.2013.02.016 Elsevier: 184–94.
[28] P.I. Teixeira, M. Warner, Dynamics of soft and semisoft nematic elastomers, Phys. Rev. E: Stat. Phys., Plasmas, Fluids, Relat. Interdiscip. Top. 60 (1) (1999) 603–609 http://www.ncbi.nlm.nih.gov/pubmed/11969799.
[29] Julie Diani, Bruno Fayolle, Pierre Gilormini, A review on the Mullins effect, Eur. Polym. J. 45 (3) (2009), https://doi.org/10.1016/j.eurpolymj.2008.11.017 Elsevier Ltd: 601–12.
[30] Jennifer M. Boothby, Hyun Kim, Taylor H. Ware, Shape changes in chemoresponsive liquid crystal elastomers, Sensor. Actuator. B Chem. 240 (2017), https://doi.org/10.1016/j.snb.2016.09.004 Elsevier B.V.: 511–18.
[31] Daniel R. Merkel, Nicholas A. Traugutt, Rayshan Visvanathan, Christopher M. Yakacki, Carl P. Frick, Thermomechanical properties of monodomain nematic main-chain liquid crystal elastomers, Soft Matter 14 (29) (2018), https://doi.org/10.1039/C8SM01178H Royal Society of Chemistry: 6024–36.
[32] Mohand O. Saed, Amir H. Torbati, Devatha P. Nair, Christopher M. Yakacki, Synthesis of programmable main-chain liquid-crystalline elastomers using a two-stage thiol-acrylate reaction, JoVE 107 (2016), https://doi.org/10.3791/53546 (January).
[33] Mohand O. Saed, Amir H. Torbati, Chelsea A. Starr, Rayshan Visvanathan, Noel A. Clark, Christopher M. Yakacki, Thiol-acrylate main-chain liquid-crystalline elastomers with tunable thermomechanical properties and actuation strain, J. Polym. Sci. B Polym. Phys. 55 (2) (2017) 157–168, https://doi.org/10.1002/polb.24249.
[34] Mohand O. Saed, Ross H. Volpe, Nicholas A. Traugutt, Rayshan Visvanathan, Noel A. Clark, Christopher M. Yakacki, High strain actuation liquid crystal elastomers via modulation of mesophase structure, Soft Matter 13 (2017), https://doi.org/10.1039/C7SM01380A Royal Society of Chemistry: 7537–47.